BASELINE DESIGN OF THE DEEP TURBINE INSTALLATION-FLOATING, A NEW FLOATING WIND CONCEPT

Jordi Serret[†1], Tahsin Tezdogan[2], Tim Stratford[1], Philipp R. Thies[3], Vengatesan Venugopal[1]

[1]University of Edinburgh, Edinburgh, UK
[2]University of Strathclyde, Glasgow, UK
[3]University of Exeter, Penryn, UK

ABSTRACT

This paper presents the preliminary design of the Deep Turbine Installation-Floating (DTI-F) concept. The DTI-F concept is a hybrid spar buoy-based floating offshore substructure capable of supporting a 7MW wind turbine with the uniqueness of being able to raise and lower the tower and nacelle, which simplifies construction, installation, maintenance, and decommissioning.

A relevant subset of design load cases (DLCs) derived from the International Electrotechnical Commission (ICE) standards is simulated with NREL-FAST software, and the aero-elastic loads are used for the structural assessment.

The paper presents the principal dimensions and crucial hydrostatic and hydrodynamic properties. The floating platform with three different mooring configurations is designed using ANSYS AQWA software, and the design is validated with experiments in laboratory conditions. The paper evaluates the design regarding the natural frequencies and the stability of the platform for a chosen site off the Scottish coast.

Further, a novel construction method, the materials chosen for the construction, and the installation and assembly processes are also outlined.

1. INTRODUCTION

In 2016, the European Commission published a review of the Renewable Energy Directive to ensure that at least 27% of the final energy consumption within the European Union comes from renewable sources by 2020. In June 2018, the European Commission has raised its target on renewable energy consumption up to 32% by 2030 [1].

European countries own extensive lands with wind conditions enough to produce wind energy at competitive costs. However, production sites are far away from demand and cause conflicts with other land users. Onshore wind is coming under greater public criticism as local governments are turning down developments. Despite that, wind energy production led the renewable mix input in 2017 [2], and offshore wind in deeper water will be an increasing source of renewable energy over the next few years [3].

This situation represents a boost for offshore wind and especially for floating wind, as this technology places the turbines far away from the shore. The better quality of the wind resource and environmental considerations will encourage developers further offshore, and floating wind turbines are set to become an attractive solution.

Over the last few years, experience has been gained with floating wind technology. It has evolved from being an academic topic to start delivering sustainable, reliable and supply energy to the grid. Equinor's Hywind project [4] installed their first full-scale spar buoy floating offshore wind turbine (FOWT) back in 2009 in the North Sea, which became in 2018 the world's first floating wind farm producing electricity to the Scottish grid. [5].

Hitherto, different floating foundations have been proposed [6, 7]. Semi-submersibles [8, 9], barges [10], and tension leg platforms [11, 12] have been developed along with spar buoy-based [13] developments like the DTI-F foundation.

This study aims to derisk the DTI-F concept further using numerical simulations validated by hydrodynamic testing, although the primary objective of this paper is to present a reliable and cost-effective solution to the wind industry.

2. DTI-F CONCEPT DESCRIPTION

The Deep Turbine Installation-Floating (DTI-F) concept is a hybrid spar buoy-based floating offshore substructure developed by Floating Wind Turbines Ltd. It consists of two cylindrical and concentric walls joined by stiffener walls.

The outer structure is composed of a 15 m diameter cylinder that increases up to 30 m in diameter by means of a frustum-cone type structure, as depicted in Figs. 1 and 2. Below the wider cylinder, a 40 m diameter water-entrapment heave plate that provides additional hydrodynamic inertia to the floater.

[†] Contact author: J.Serret@ed.ac.uk

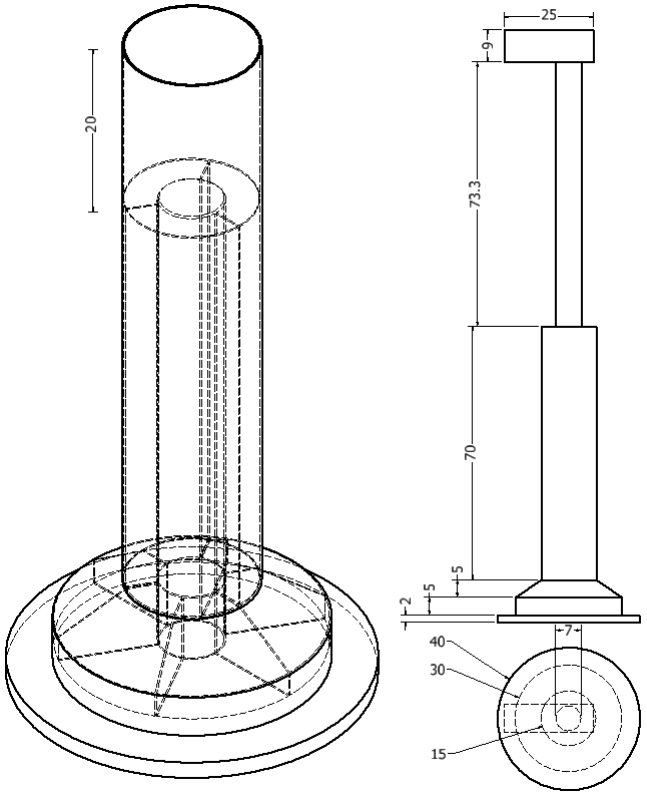

FIGURE 1: DTI-F SUBSTRUCTURE (LEFT) AND COMPLETE SYSTEM (RIGHT) WITH DIMENSIONS IN METERS.

The inner structure of the floater is composed of another hollow cylinder, 7 m in diameter. This hollow cylinder goes from the draft line to the bottom of the structure. The space between the two cylinders at the top provides the necessary buoyancy to the floater. The void space in the wider cylinder at the bottom is used to store the ballast water. This deposit, i.e. the wider cylinder, has different sealed tanks and stiffener walls for structural reinforcement. Both the inner and wider cylinders are connected at the bottom end of the floater, allowing the tower and nacelle set to be raised and lowered down within the inner cylinder by flooding them using the ballast water (Fig. 2). A 30 m height flotation cylinder, designed to counteract the weight of the tower and the nacelle, is installed at the bottom of the tower. This flotation cylinder is a critical component that allows both the tower and nacelle to float.

An active ballast system transfers water from the wider cylinder to the inner hollow cylinder to float the tower and nacelle set, allowing it to be raised and lowered, avoiding the use of expensive cranes during installation, maintenance and decommissioning processes.

The substructure has four boat landing areas, serviced by two remotely controlled lifts, ensuring at least one sheltered access point regardless of the wave direction.

A total of 553 m^2 of deck space located 20 m above the sea-level to avoid splashing waves, will give access to the facilities located within the substructure. It includes elevator accesses, a workshop, machinery rooms, structural tendons inspection access space, winches control room, and IT and communications space among others.

The floating substructure is designed to carry a standard 7 MW offshore wind turbine. However, the initial design is flexible enough to operate with offshore wind turbines up to 15 MW with suitable modifications, i.e. increasing thickness of the walls, increasing the reinforcement capacity, increasing installation depth.

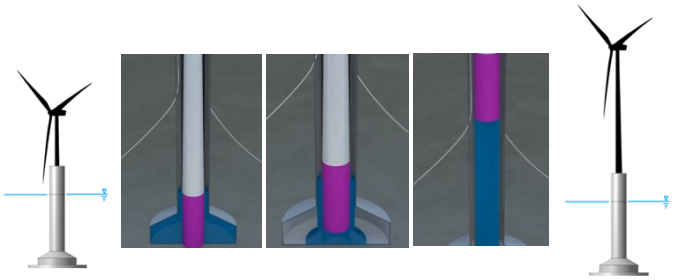

FIGURE 2: RAISING MECHANISM SEQUENCE USING THE FLOTATION CYLINDER ALONG WITH THE BALLAST WATER TO FLOAT UP THE TOWER AND NACELLE SET.

3. SITE CONDITIONS

The DTI-F design is strongly site-dependent. The most relevant site-related parameter for the design is the installation depth. The site chosen for the evaluation of the design presented in this paper is the Buchan Deep site in the vicinity of the Hywind test site. This site is selected because of the availability of data and environmental conditions [14, 15, 16]. The site is depicted in Fig. 3.

The location has a range of depths between 90 and 120 m depth, dominated by waves coming from the North and South-West with operational significant wave heights up to 4 m and peak wave periods up to 8 s. Extreme wave models [14] forecast a one-year return period wave with a significant height of 15.2 m and 11.2 s period, while the values increase until 17.8 m and 12.2 s, and 19.7 m and 12.8 s for ten, and fifty-year return periods, respectively.

The primary North Sea tides travel from North to South and then is reflected off to the North again. As a semi-diurnal tide, flood and ebb phases are flowing parallel to the shore. The spring tidal range is approximately 3.8 m, and the neap is 3.1 m. At 60 m depth in Buchan Deep, the mean tidal current speed is approximately 0.37 ms^{-1} with maximum speeds of 1.27 ms^{-1} during spring tides, whereas at 25 m depth the mean speed is 0.40 ms^{-1} with maximum speeds of 1.42 ms^{-1} [17].

Wind speeds are provided by the Nora10 forecast model [18] operated by the Norwegian Meteorological Institute using wind data from 1980 to 2010, which are extrapolated at the height of 100 m above sea level. The model hindcast provides average wind speed values between 8 and 13 ms^{-1}, maximum wind speed values between 20 and 35 ms^{-1}, and turbulence intensity of 0.05 for wind speeds of 10 ms^{-1} at 100 m above the sea level. The wind direction is predominantly South-Westerly.

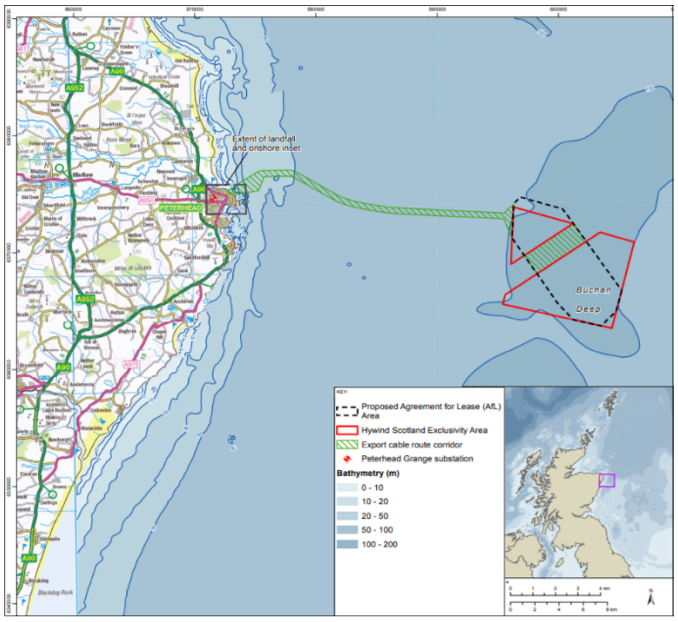

FIGURE 3: BUCHAN DEEP SITE LOCATION [17]

The seabed at Buchan Deep contains superficial deposits of Holocene sands in the form of less than 0.5 m thick layers. Below, quaternary soils up to 40 m thick directly overlying the basement bedrock [15].

This location represents the shallower installation limit for this hybrid spar buoy-based concept. Consequently, it challenges the design and compromises the maximum cost reductions. Evidently, the deeper the installation site is, the bigger the draft of the substructure can be designed. Therefore, the height of the cranes required for installation, maintenance, and decommission decreases, along with the associated costs.

4. WIND TURBINE DESIGN

Existing floating concepts in academic studies are predominantly based on reference turbines (e.g. NREL-5MW, DTU-10MW) instead of commercial turbines. However, even well-matured projects, such as Hywind, with real prototypes working on the sea, were initially based on reference wind turbines and then were scaled up or down as required [19].

The development of the DTI-F has been based on a 7MW foreshore wind turbine from the outset. The Levenmouth wind turbine is owned by Offshore Renewable Energy Catapult and dedicated to research purposes. The main properties of the Levenmouth turbine are given in Fig. 4 [20].

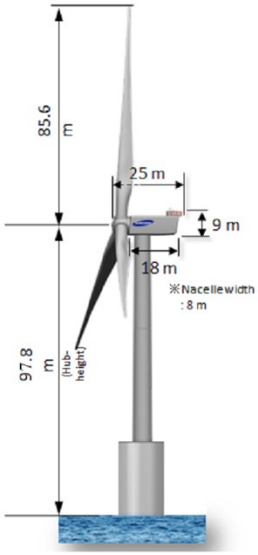

Wind Class	IEC Class 1A
Rotor diameter	171.2 m
Capacity	7 MW
Hub height	110.6 m
Blade length	83.5 m
Generator	Medium (3.3kV), PMG
Converter	Full power conversion
Drivetrain	400 rpm
Rated frequency	50 Hz
Rotor speed	5.9 – 10.6 rpm
Wind speed	3.5 – 25 ms^{-1}
Rated wind speed	10.9 ms^{-1}
Design life	25 years
Certification	DNV
Control System • Independent and collective pitch control modes • Active drive train damping • Active load control • Blade load monitoring	

FIGURE 4: LEVENMOUTH WIND TURBINE CHARACTERISTICS [20]

The calculation of the loads coming from the interaction between wind and blades, transmitted through the shaft, equalised by the controller, transmitted to the tower, and eventually distributed through the foundation, are critical to ensuring the structural integrity of the floating platform. To calculate these aero-servo-elastic loads, NREL FAST has been the tool of choice. NREL FAST [21] is a glue code coupling results from different simulators and pre-processors. Finally, these aero-servo-elastic loads must be coupled with the hydrodynamic loads to capture the complex behaviour of floating wind turbines. Further explanation of the modelling tool, the simulations carried out, the complete description of the model, limitations, and results are discussed in [20]. Table 1 presents the diagonal of the ultimate limit state-load matrix obtained by NREL FAST and Fig. 5 and 6 show the steady-state simulation results. It should be noted that the results of the aeroelastic simulation are given without magnitudes to protect ORE Catapult's / Samsung's proprietary information.

TABLE 1: DIAGONAL OF THE ULTIMATE LIMIT STATE-LOAD MATRIX FOR THE LEVENMOUTH WIND TURBINE [20]

	M_x (kNm)	M_y (kNm)	M_z (kNm)	F_x (kN)	F_y (kN)	F_z (kN)
Max	42625	149050	19062	2430	527	-8514
Min	-40689	-248270	-19346	-2522	-543	-11421

Figure 5 presents the most relevant steady-state results [20] for the Levenmouth offshore wind turbine. Steady-state results show the behaviour of different sub-systems, e.g. generator, controller, for a set of non-turbulent input winds. Therefore, these results are convenient to characterise the functionality of a wind turbine.

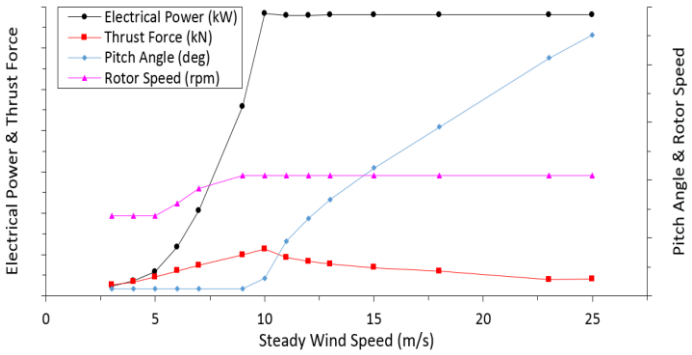

FIGURE 5: STEADY-STATE RESULTS OF THE LEVENMOUTH WIND TURBINE

Figure 6 shows the power coefficient versus the tip speed ratio for a set of steady wind velocities. It shows good agreement of the NREL FAST simulation with the commissioning results of the Levenmouth wind turbine [20].

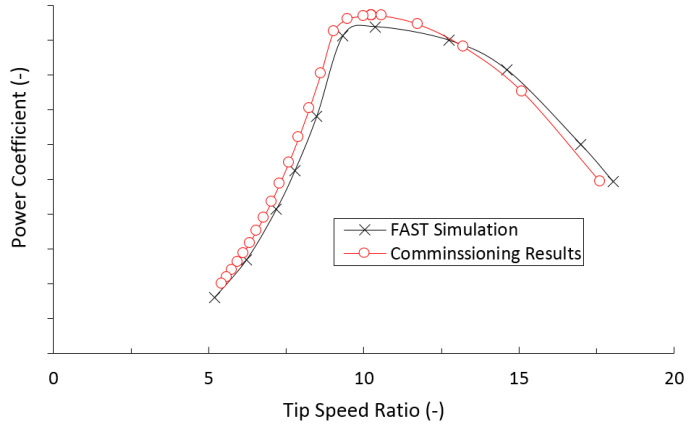

FIGURE 6: POWER COEFFICIENT VS TIP SPEED RATIO FOR THE LEVENMOUTH WIND TURBINE

5. PLATFORM DESIGN

The DTI-F platform is a spar buoy-based concept. Spar buoys have a deep draft minimising vertical wave forces and therefore vertical modes motion. The deep draft allows for low centre of gravity designs ensuring big righting moments, and consequently low pitch and roll modes of motion.

Three different catenary mooring configurations have been proposed for the seakeeping of the DTI-F concept, i.e. (i) three lines distributed at 120 degrees, (ii) four lines distributed at 90 degrees, and (iii) three lines distributed at 120 degrees with a delta connection (Fig. 7). The four lines configuration has been tested to investigate surge and sway motion reductions whereas the delta connection configuration has been tested to explore the yaw rotation motion reduction.

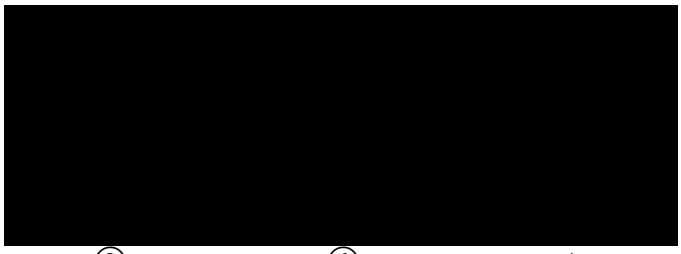

FIGURE 7: MOORING LAYOUT

Shapes and dimensions have been chosen to fulfil functional requirements included in floating structures recommended practices [22]. Keeping the natural periods of the structure away from the periods of excitation as well as controlling the global motions, are the main design criteria.

Table 2 presents a new analysis of the natural periods and damping coefficients presented in [23]. Damping coefficients and natural periods of oscillation for the three different mooring line configurations are expressed as full-scale equivalent values.

TABLE 2: RESONANCE PROPERTIES OF THE DTI-F SYSTEM FOR THE THREE DIFFERENT MOORING CONFIGURATIONS

	Damping coefficient (-)			Natural period (s)		
Mooring setup	③	Δ	④	③	Δ	④
Heave	4×10^{-3}	4×10^{-3}	4×10^{-3}	28	28	28
Surge	2×10^{-3}	2×10^{-3}	2×10^{-3}	169	169	169
Sway	*	*	*	*	*	*
Pitch	1×10^{-3}	8×10^{-4}	1×10^{-3}	88	55	50
Roll	1×10^{-3}	8×10^{-4}	1×10^{-3}	91	55	49
Yaw	1×10^{-3}	5×10^{-3}	2×10^{-3}	121	42	70
* Inconclusive results						

The natural period results show that all six degrees of freedom are longer than the linear wave excitation, as the ocean waves contain first harmonic wave energy in the period range of 5 - 25 seconds [23].

For a spar buoy-based FOWT the natural periods in surge, sway and yaw should be larger than 100 seconds, 20-35 seconds for heave, and 50-90 seconds for roll and pitch [22]. Therefore, the results meet the constraints specified in the relevant standards.

Comparing the results to the Equinior's (formerly Statoil) Hywind project results [13], the DTI-F concept has a 25% longer surge period, a similar heave period, a 75% longer pitch and roll periods, and a 95% longer yaw period.

Regarding the global motions, the following limitations have been considered to ensure the proper operability of the wind turbine:

- the amplitude of the roll and pitch rotational modes of motion must remain under 10 degrees [24]; and
- the induced maximum horizontal acceleration at the nacelle must be kept under 3ms^{-2} [25].

5.1 Construction material

Most of the prototypes developed for FOWT are made of steel. Steel has favourable mechanical properties, but the cost of the material and the expensive maintenance required in marine environments prevents it from being a cost-effective choice.

On the other hand, concrete has been proven a reliable [26] and cost-effective solution since the 70s when the first concrete platforms were installed in the North Sea. Since then the properties of concrete have been improved. Higher strength mixtures with lower permeability have been developed giving the opportunity for concrete marine structures to increase their lifetime and reduce their operations expenditure (OPEX).

Concrete is also cheaper than steel [27], allowing for further reductions in construction costs and therefore the capital expenditure (CAPEX).

However, durability and fatigue-related problems have been recorded by the offshore wind industry in the concrete-steel interface of fixed-bottom offshore wind farms.

Even though the durability and fatigue problems in the concrete-steel interface introduce some design challenges, concrete is the material of choice. However, the details regarding the concrete mix still cannot be reported since they are under investigation.

5.2 Structural relevant details

Concrete works well in compression, but not in tension. Therefore, the substructure must always be kept in compression. To maintain compression along the substructure, the precast modules will be post-tensioned using steel tendons. Tendons are installed through duct pipes in the precast modules, stressed, and sealed. To stress the tendons, post-tensioning anchors are placed between each of the precast modules, and between the top of the substructure and the bottom, i.e. heave plate.

The structure also has passive reinforcement consisting of both, randomly dispersed fibres in the cement mix and corrosion protected rebar, e.g. epoxy coated or stainless rebar.

The structural integrity of the floater is also under analysis. Therefore, neither the amount nor grade of the steel nor the composition or distribution of the fibres can be disclosed.

5.3 Hydrostatic and hydrodynamic properties of the floater

The hydrostatic properties of the DTI-F substructure without moorings have been calculated using ANSYS AQWA, a widely used diffraction software using potential flow theory.

Figure 8 shows the mesh used by the diffraction code to calculate volumes and stiffness. Even though the tower, nacelle, and blades are not represented in the geometry, their effect has been modelled having them into account in the mass distribution.

The optimal density of the mesh must allow fitting seven-panel sizes in one wavelength. For the present study, the results converge for a mesh with a maximum element size of 1 m. However, since the size of the mesh also defines the maximum allowed frequency, the size of the panels has been set up at 0.66 m to increase the range of frequencies considered in this study.

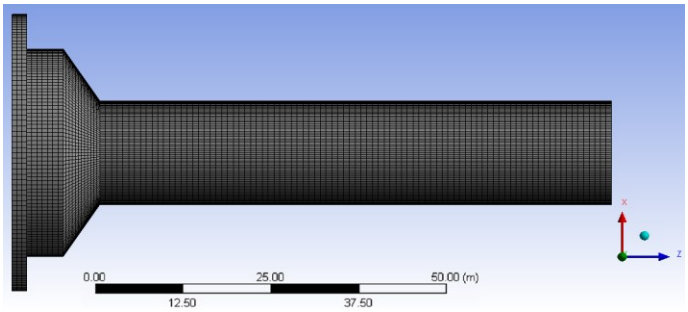

FIGURE 8: MESH USED BY THE DIFFRACTION CODE

The main hydrostatic parameters are shown in Table 3 along with mass and inertia properties. The height of the centre of gravity (CoG), the centre of buoyancy (CoB), and the moments of inertia are calculated from the bottom of the structure.

The most relevant parameter in Table 3 is the CoB to metacentre distance. This distance must be positive in floating structures in order to be stable. However, it should be kept as small as possible since small CoB to metacentre distances imply a tender floating structure with more significant roll periods ensuring a smoother operation of the wind turbine.

TABLE 3: HYDROSTATIC, MASS, AND INERTIA PROPERTIES OF THE DTI-F IN THE FREE-FLOATING POSITION

Volumetric displacement (m^3)	1.69×10^4
Draft (m)	62.00
Total mass (kg)	1.70×10^7
Centre of gravity (CoG) height (m)	20.13
Centre of buoyancy (CoB) height (m)	21.47
Metacentric height (m)	21.62
Principal 2nd moments of area (m^4)	2.48×10^3
CoB to metacentre (m)	0.15
X moment of inertia (kgm^2)	2.14×10^{10}
Y moment of inertia (kgm^2)	2.14×10^{10}
Z moment of inertia (kgm^2)	1.9×10^9

The heave (C_{33}), roll (C_{44}), and pitch (C_{55}) hydrostatic stiffness coefficients measured from the CoG, and their corresponding computed natural periods of oscillation (T_3), (T_4), and (T_5) are presented in Table 4.

TABLE 4: HEAVE, ROLL, AND PITCH HYDROSTATIC STIFFNESS COEFFICIENTS AND NATURAL PERIODS OF OSCILLATION OF THE DTI-F IN THE FREE-FLOATING POSITION

C_{33}	1.78×10^6 N/m	T_3	28 s
C_{44}	4.41×10^6 Nm/°	T_4	30 s
C_{55}	4.41×10^6 Nm/°	T_5	30 s

The T_3 and T_4 values shown in Table 4 are smaller than the ones presented in Table 2. As mentioned before the values in Table 4 are the natural periods of oscillation of the system without mooring lines. Once the moorings are attached to the floater, T_4 and T_5 values increase due to the line's additional stiffness. The value of T_3 is the same in Tables 4 and 2. Therefore, the mooring line does not increase the stiffness of the system in the heave mode of motion.

The hydrodynamic properties of the DTI-F substructure without moorings have also been calculated using ANSYS AQWA. The potential flow theory used by ANSYS AQWA do not includes viscous effects. Therefore, a drag coefficient of 0.6 [28] has been applied to consider them.

Experiment and numerical results for the free decay condition in heave are depicted in Fig. 9 showing good agreement.

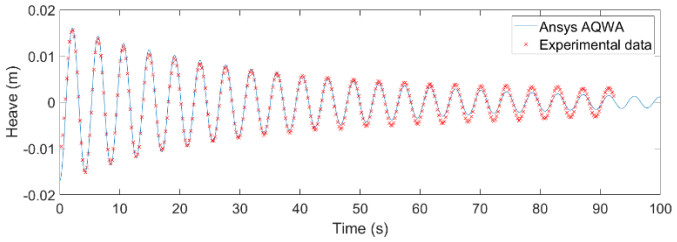

FIGURE 9: EXAMPLE OF FREE DECAY TEST IN HEAVE

The response amplitude operators, the added mass, and the radiation damping of the free floater are depicted in Figs. 10, 11, and 12 respectively.

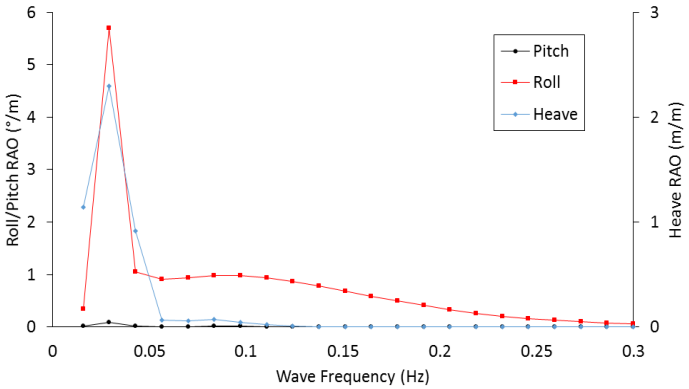

FIGURE 10: PITCH, ROLL, AND HEAVE RESPONSE AMPLITUDE OPERATORS OF THE DTI-F.

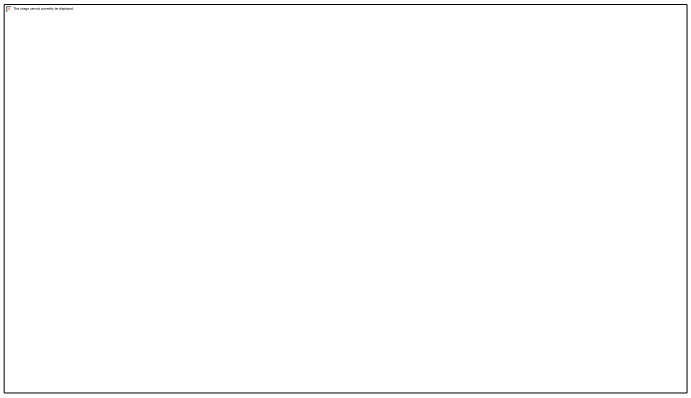

FIGURE 11: PITCH, ROLL, AND HEAVE ADDED MASS OF THE DTI-F. NOTE THAT PITCH AND ROLL ADDED MASS VALUES ARE IDENTICAL.

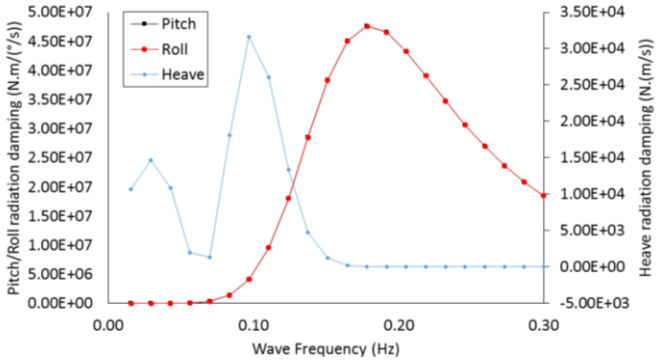

FIGURE 12: PITCH, ROLL, AND HEAVE RADIATION DAMPING OF THE FREE FLOATER. NOTE THAT PITCH AND ROLL VALUES ARE IDENTICAL.

Further hydrodynamic behaviour analysis considering the mooring lines beyond the natural periods provided in Table 2, will be the subject of future work.

5.4 Construction and deployment

The simple geometry of a spar buoy allows the use of a modular construction scheme. The precast concrete components can be fabricated off-site under controlled conditions, using simple formwork, and avoiding expensive slip forming. The reinforcement can be added in a controlled and efficient way of producing concrete precast modules. As precast concrete uses standard forms, modules can be produced in larger numbers, improving the economies of scale.

Construction will be carried out using a floating production line without the use of dry docks or similar facilities.

Figure 13 illustrates a typical site layout including a batching plant, rebar and precast modules construction yards, the substructure assembly area, and the turbine assembly area.

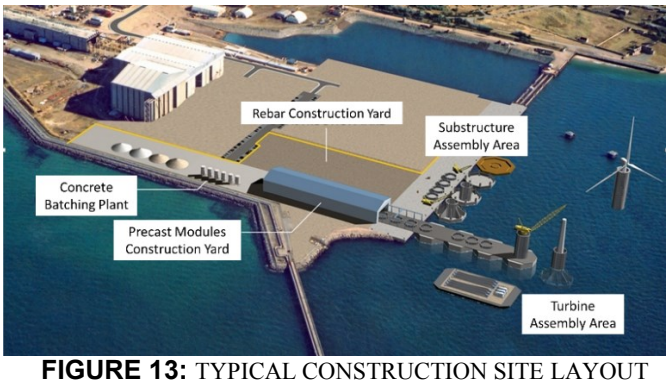

FIGURE 13: TYPICAL CONSTRUCTION SITE LAYOUT

The heave plate and the base sections are designed to be built on a submersible pontoon in shallow waters. With the base cast and afloat, precast modules are stacked along with the flotation cylinder (Fig. 14a) and the corresponding tower sections (Fig. 14b). Once the whole substructure is built, base and water ballast are added, and the substructure can be towed to a deeper assembly area (Fig. 14c). Finally, the nacelle and blades will be assembled (Fig. 14d), and the complete system can be tested at quayside to allow for troubleshooting before installation in deep waters.

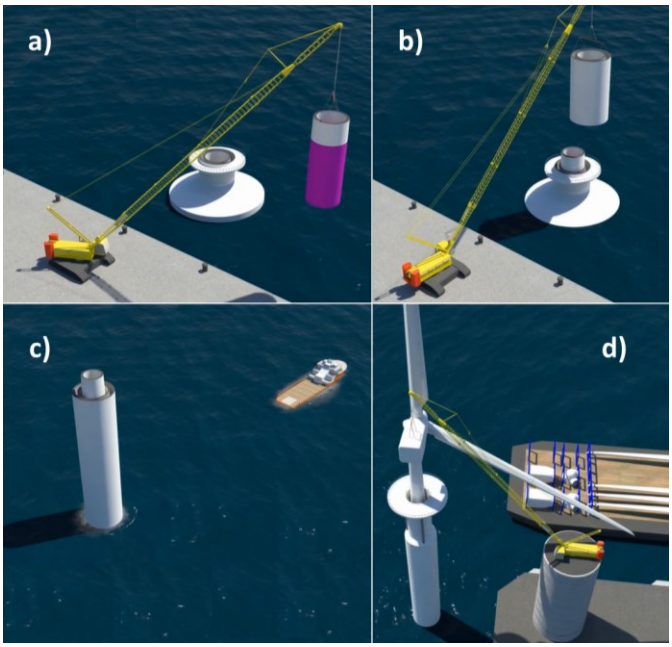

FIGURE 14: CONSTRUCTION METHOD. A) ADDITION OF THE FLOTATION CYLINDER AT THE ASSEMBLY AREA, B) ADDITION OF THE PRECAST MODULES AND TOWER SECTIONS, C) SUBSTRUCTURE TOWED TO THE TURBINE ASSEMBLY AREA, AND D) NACELLE, ROTOR AND BLADES FITTED, AND READY TO BE TESTED

Figure 15 presents the depths required at each of the different construction stages. The DTI-F substructure requires less than 10 m depth for the early stages of the building and from 10 to 25 m depth for the complete floater construction.

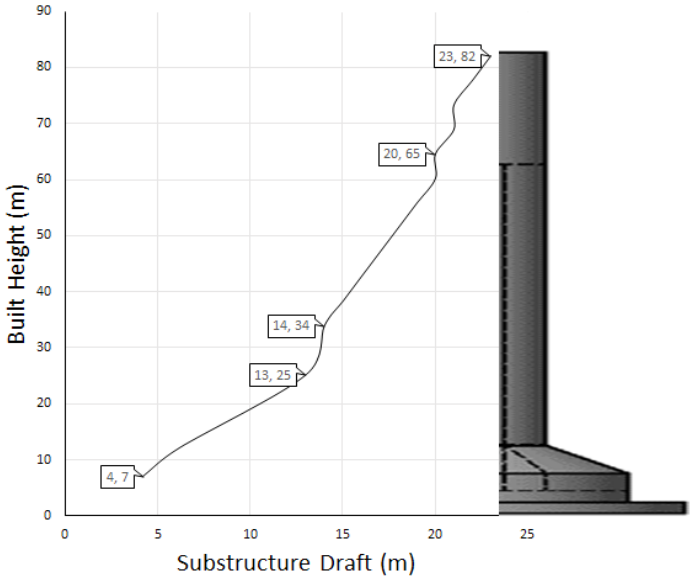

FIGURE 15: NEEDED DRAUGHT DURING CONSTRUCTION

Figure 16 presents the draught requirements from the assembly phase to the commissioning stage. It includes the addition of the base ballast, the fitting of the nacelle, the rotor, the blades and the transfer of the ballast water until the full commissioning of the system with the tower erected and the turbine ready to be tested.

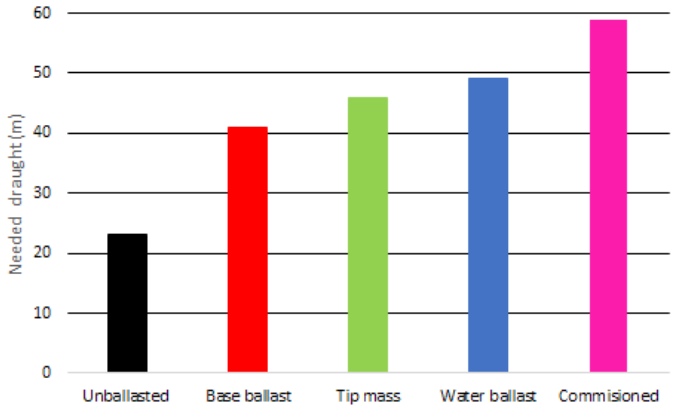

FIGURE 16: DRAUGHT REQUIRED TO DELIVER THE SUBSTRUCTURE

6. DISCUSSION

This study presents the first iteration design of the DTI-F. The DTI-F system lays on the use of concrete for the floater as a measure to reduce the CAPEX since the price of concrete is two orders of magnitudes lower than steel prices. The construction method gathers prefabricated concrete modules with a floating production line resulting in an even greater reduction of CAPEX. With a very low level of maintenance required, it is also a key factor to reduce OPEX.

However, the most relevant factor regarding the reduction of OPEX is related to the installation and maintenance processes. Installation and maintenance processes of the DTI-F system are improved by the possibility of raising and lowering the tower and nacelle set multiple times. Other concepts like the Steyco [29] self-installing precast concrete telescopic tower and foundation benefits of cost reductions during installation, but not during maintenance as they are no able to lower tower and nacelle after they are raised when installed.

The natural periods of the floating system are removed from the typical range of wave periods, and response amplitude operators, added mass, and radiation damping values are in the range expected for a spar buoy.

The frequency domain statistic results show extreme pitch rotational amplitudes of 4.18°, with induced acceleration on the order of 0.4 ms^{-1} at the nacelle. Negligible values were found for the roll mode of motion.

The main assumption regarding the design was made for the transmission/clamping piece. It has been left out of this work, and only an estimation of the weight has been developed for the present study.

Another important assumption made in the calculations is related to the potential flow theory used by ANSYS AQWA since it does not include viscous effects. However, widely accepted drag coefficients have been included to account for that limitation.

7. CONCLUSIONS AND RECOMMENDATIONS

The baseline design of the DTI-F system has been carried out using a concrete spar buoy-based floater supporting the Levenmouth wind turbine (7MW). The results are a good indication that the fundamental design of the concept is technically feasible.

The design has been analysed for a site representing the shallower installation option. Therefore, since the deeper the installation site is, the more significant will crane cost reduction be.

ANSYS AQWA results show good agreement with experimental data, accurately reproducing natural frequencies and dynamic behaviour.

Installation and construction methods have been designed to minimise offshore operations. The raising mechanism allows for installation and maintenance avoiding the use of heavy lifting cranes.

Further optimisation of the system can be achieved by using a two-bladed wind turbine. Two-bladed wind turbines exhibit lower power performance than a three-bladed wind turbine. However, the cost reduction in materials along with a slightly longer blade will counteract this lower power output. Besides, the two-bladed wind turbine geometry allows lowering the nacelle with the blades in horizontal position. Therefore, the installation and maintenance operations can be performed only at 20 meters above the sea level which has the potential to impact the OPEX and the global cost of the energy advantageously.

ACKNOWLEDGEMENTS

This work is funded in part by Floating Wind Turbines Limited (FWT Ltd), and the Energy Technologies Institute (ETI); Research Councils UK (RCUK); Energy Programme for the Industrial Doctorate Centre for Offshore Renewable Energy (IDCORE) [grant number EP/J500847/1].

The aeroelastic model of the Levenmouth wind turbine is based on the data kindly provided by Offshore Renewable Energy (ORE) Catapult.

The testing data has been produced thanks to MaRINET2 support. European Union's Horizon 2020 research and innovation programme under grant agreement number 731084.

REFERENCES

[1] European Commission (2018). Renewable energy: Moving towards a low carbon economy. [online] Available at: https://ec.europa.eu/energy/en/topics/renewable-energy [Accessed 4 Sep. 2018].

[2] BP plc (2018). Statistical Review of World Energy 2018 [online] Available at: https://www.bp.com/content/dam/bp/en/corporate/pdf/energy-economics/statistical-review/bp-stats-review-2018-full-report.pdf [Accessed 4 Sep. 2018].

[3] ORE Catapult (2018). Floating wind: technology assessment. [online] Available at: https://ore.catapult.org.uk/app/uploads/2018/01/Floating-wind-technology-assessment-June-2015.pdf [Accessed 4 Sep. 2018].

[4] Equinor.com. (2018). Our offshore wind projects - Our offshore wind projects - equinor.com. [online] Available at: https://www.equinor.com/en/what-we-do/new-energy-solutions/our-offshore-wind-projects.html [Accessed 20 May 2018].

[5] Equinor.com. (2018). World's first floating wind farm has started production - World's first floating wind farm has started production - equinor.com. [online] Available at: https://www.equinor.com/en/news/worlds-first-floating-wind-farm-started-production.html [Accessed 4 Sep. 2018].

[6] The Carbon Trust (2015). Market and Technology Review. Floating Offshore Wind. [online] Available at: https://www.carbontrust.com/media/670664/floating-offshore-wind-market-technology-review.pdf [Accessed 20 May 2018].

[7] European Wind Energy Association (2013). Deep Water. The next step for offshore wind energy. [online] Available at: http://www.ewea.org/fileadmin/files/library/publications/reports/Deep_Water.pdf [Accessed 20 May 2018].

[8] Paulsen, U., Vita, L., Madsen, H., Hattel, J., Ritchie, E., Leban, K., Berthelsen, P. and Carstensen, S. (2012). 1st DeepWind 5 MW Baseline design. Energy Procedia, 24, pp.27-35.

[9] Lefebvre, S. and Collu, M. (2012). Preliminary design of a floating support structure for a 5MW offshore wind turbine. Ocean Engineering, 40, pp.15-26.

[10] Borisade, F., Choisnet, T. and Cheng, P. (2016). Design study and full scale MBS-CFD simulation of the IDEOL floating offshore wind turbine foundation. Journal of Physics: Conference Series, 753, p.092002.

[11] Oguz, E., Clelland, D., Day, A., Incecik, A., López, J., Sánchez, G. and Almeria, G. (2018). Experimental and numerical analysis of a TLP floating offshore wind turbine. Ocean Engineering, 147, pp.591-605.

[12] Adam, F., Myland, T., Dahlhaus, F. and Großmann, J. (2015). GICON®-TLP for wind turbines – the path of development. Renewable Energies Offshore, pp.651-656.

[13] Driscoll, F., Jonkman, J., Robertson, A., Sirnivas, S., Skaare, B. and Nielsen, F. (2016). Validation of a FAST Model of the Statoil-hywind Demo Floating Wind Turbine. Energy Procedia, 94, pp.3-19.

[14] Xodus Group Ltd (2013). Hywind Scotland Pilot Park Project. EIA Scoping Report.

[15] Statoil (2015). Hywind Scotland Pilot Park. Environmental Statement.

[16] Statoil (2014). Hywind Buchan Deep Metocean Design Basis. Revision 2. May 2014. Document number: RE2014- 002.

[17] UKHO (2013). North Sea Pilot (West). NP 54. 9th Edition.

[18] Reistad, M, Breivik, Ø, Haakenstad, H, Aarnes, O J, Furuvik, B R and Bidlot, J R (2011), A high resolution hindcast of wind and waves for the North Sea, Norwegian Sea, and the Barents Sea, Journal of Geophysical Research, 116, C05019, DOI: 10.1029/2010JC006402. [online] Available at: http://onlinelibrary.wiley.com/doi/10.1029/2010JC006402/suppinfo

[19] Shin, H. (2011). Model Test of the OC3-Hywind Floating Offshore Wind Turbine. Maui, Haway, USA: Proceedings of the 21st International Offshore and Polar Engineering conference.

[20] Serret, J., Rodriguez, C., Tezdogan, T., Stratford, T., Thies, P.R. (2018). Code comparison of a NREL-FAST model of the Levenmouth wind turbine with the GH Bladed commissioning results. Proceedings of the ASME 2018 37th International Conference on Ocean, Offshore and Arctic Engineering. DOI: 10.1115/OMAE2018-77495. [online] Available at: http://proceedings.asmedigitalcollection.asme.org/solr/searchresults.aspx?q=OMAE2018-77495&f_ContentType=Proceedings&SearchSourceType=3

[21] Jonkman, J. and Buhl, M. (2005). FAST user's guide. 1st ed. Golden, Colorado: National Renewable Energy Laboratory.

[22] DNV Recommended Practice DNV-RP-F205, Global Performance Analysis of Deepwater Floating Structures, October 2010.

[23] Serret, J., Tezdogan, T., Stratford, T., Thies, P.R. and Venugopal, V. (2018). Model test of the DTI-Floating wind concept. Proceedings of the 3rd International Conference on Offshore Renewable Energy. [online] Available at: https://strathprints.strath.ac.uk/65393/1/Serret_etal_CORE2018_Model_test_of_the_DTI_Floating_wind_concept.pdf [Accessed 15 Oct. 2018].

[24] T. Zambrano, T. MacCready, T. Kiceniuk, D. Roddier, C.Cermelli, ”Dynamic Modeling of Deepwater Offshore Wind Turbine Structures in Gulf of Mexico Storm Conditions”, OMAE 2006, Hamburg, Germany

[25] Ramachandran, G., Vita, L., Krieger, A. and Mueller, K. (2017). Design Basis for the Feasibility Evaluation of Four Different Floater Designs. Energy Procedia, 137, pp.186-195.

[26] FIP (1996). State of the art report: Durability of concrete structures in the North Sea. London, SETO.

[27] Campos, A., Molins, C., Gironella, X. and Trubat, P. (2016). Spar concrete monolithic design for offshore wind turbines. Proceedings of the Institution of Civil Engineers - Maritime Engineering, 169(2), pp.49-63.

[28] Chakrabarti, S. (2005). Handbook of offshore engineering. Amsterdam: Elsevier.

[29] Esteyco (2016). Self-installing precast concrete telescopic tower and foundation. [online] Available at: http://www.esteyco.com/projects/elican/wp-content/uploads/2018/01/Poster_AWEA-Offshore_Warwik-2016.pdf [Accessed 2 Nov. 2018].